frontiers | Frontiers in Earth Science

ORIGINAL RESEARCH
published: 09 August 2022
doi: 10.3389/feart.2022.940205

Lightning Distribution in Tropical Cyclones Making Landfall in China

Wenjuan Zhang[1], *Yijun Zhang*[2,3,4]*, *Shoujuan Shu*[5], *Dong Zheng*[1] *and Liangtao Xu*[1]

[1]State Key Laboratory of Severe Weather, Chinese Academy of Meteorological Sciences, Beijing, China, [2]Department of Atmospheric and Oceanic Sciences and Institute of Atmospheric Sciences, Fudan University, Shanghai, China, [3]CMA-FDU Joint Laboratory of Marine Meteorology and Shanghai Frontiers Science Center of Atmosphere-Ocean Interaction, Shanghai, China, [4]Shanghai Qi Zhi Institute, Shanghai, China, [5]Department of Atmospheric Sciences, School of Earth Sciences, Zhejiang University, Hangzhou, China

Lightning data from the World Wide Lightning Location Network (WWLLN) are used to document the lightning characteristics in tropical cyclones (TCs) making landfall in China. The landfall period is confined to 48 h prior to and after landfall (t_{-24}~t_{+24}). Data from a total of 74 TCs are collected from 2010 to 2020, providing 3,293 individual time periods (1-h periods). To examine the radial and asymmetry distributions as a function of TC intensity, landing location, and vertical wind shear, the dataset is classified into two intensity categories, three shear groups, and four landing locations. WWLLN detected lightning activity in all TCs during the 48-h landfall, with lightning rates most frequently appearing between 250 and 600 str h^{-1}. Extreme hourly lightning rates of 3,154 str h^{-1} and 4,426 str h^{-1} are observed in the inner core in Tropical Storm Cimaron (2013) and the outer rainbands in Severe Typhoon Matmo (2014), respectively, comparable to lightning activity in mesoscale convection systems on land. TCs landing in Guangdong and Hainan have the largest peak lightning rates, while those landing in Zhejiang and Shanghai show the lowest lightning rates. The maximum lightning density is found in the inner-core region of weak TCs (<32.7 m s^{-1}) that are located approximately 100–200 km away from the coastline. The radial distribution of lightning density at landing stages is consistent with that at mature stages when TCs are over the ocean. However, there is a shift in the lightning maximum from the inner core prior to landfall (t_{-24}~t_0) to the outer rainbands after landfall (t_0~t_{+24}), indicating the effects of dry continental air intrusion and the enhanced surface frictional convergence. Vertical wind shear is the dominant factor in producing lightning and convective asymmetry for TCs landing in all locations. Lightning asymmetries are enhanced with the increase in shear magnitude from low (<5 m s^{-1}) to moderate (5–10 m s^{-1}) and high (>10 m s^{-1}) shear environments, both in weak and strong TCs (≥32.7 m s^{-1}).

Keywords: lightning, convection, tropical cyclone, landfall, China

OPEN ACCESS

Edited by:
Dujuan Kang,
Rutgers, The State University of New Jersey, United States

Reviewed by:
Jilong Chen,
The Chinese University of Hong Kong, China
Qiaoyan Wu,
Ministry of Natural Resources, China

***Correspondence:**
Yijun Zhang
zhangyijun@fudan.edu.cn

Specialty section:
This article was submitted to Atmospheric Science, a section of the journal Frontiers in Earth Science

Received: *10 May 2022*
Accepted: *09 June 2022*
Published: *09 August 2022*

Citation:
Zhang W, Zhang Y, Shu S, Zheng D and Xu L (2022) Lightning Distribution in Tropical Cyclones Making Landfall in China. Front. Earth Sci. 10:940205. doi: 10.3389/feart.2022.940205

1 INTRODUCTION

The northwest Pacific is the most active tropical cyclone (TC) basin (Gray, 1968) in terms of genesis, intensity and landfall events. The frequent disasters caused by landing TCs pose a significant threat to human life and property in China. One of the most serious disasters is heavy rainfall, which causes widespread flooding over coastal areas. For example, Typhoon Morakot affected much of China's

southeast coast during August 2009. Extreme rainfall of 1623.5 mm was recorded in 24 h at stations located in Fujian and Taiwan, causing an estimated 789 deaths and economic losses of 6.2 billion dollars (Chien and Kuo, 2011; Chen and Xu, 2017). Therefore, knowing the specific location of heavy rainfall during TC landfall is crucial for disaster reduction.

The heavy rainfall in TCs is related not only to the large-scale environments but also to the vortex structure and its cloud microphysical process (Houze, 2010). Intense convective cells are usually responsible for the maxima of TC rainfall near the coastline (Chan et al., 2004). A numerical study on Typhoon Morakot (2009) indicates that ice-phase processes and the large number of ice particles and graupels generated in deep convection in the rainbands are responsible for the extreme rainfall during Morakot's landfall (Chen and Xu, 2017). The ice particles transported outward by the radial wind increase the number of condensation nuclei in the stratiform region, where they melt and fall out in the form of large raindrops (Houze, 2010). Cloud electrification is closely related to microphysics, especially ice-phase processes (Williams, 1988). Therefore, the study of lightning characteristics in landing TCs can improve our understanding of TC convective distribution and its potential signals for cloud microphysical processes associated with heavy rainfall during landfall.

Over the previous few decades, a number of studies have examined the temporal and spatial distributions of lightning in TCs. Earlier studies have used lightning data from regional and national ground-based lightning detection networks, such as the National Lightning Detection Network (NLDN; Samsury and Orville, 1994; Molinari et al., 1994; Molinari et al., 1999; Molinari et al., 2004), Long-range Lightning Detection Network (LLDN; Squires and Businger, 2008; Leary and Ritchie, 2009), Los Alamos Sferics Array (LASA, Shao et al., 2005; Fierro et al., 2011), and Guangdong Lightning Location System in China (GDLLS; Zhang et al., 2012). Thanks to the remote detection of very-low-frequency electromagnetic waves over the open oceans, recent studies have used the global ground-based lightning location network, e.g., the World Wide Lightning Location Network (WWLLN; Pan et al., 2010; Thomas et al., 2010; Abarca et al., 2011; Bovalo et al., 2014; Zhang et al., 2015; Solorzano et al., 2018; Lin and Chou, 2020), Vaisala's Global Lightning Dataset (GLD360; Vagasky, 2017; Fierro et al., 2018), and Earth Networks Total Lightning Network (ENTLN; Ringhausen and Bitzer, 2021), to monitor lightning activity during the entire life cycle of TCs in different basins.

Satellite instruments, such as the Optical Transient Detector (OTD) on the Microlab-1 satellite and the Lightning Imaging Sensor (LIS) on the Tropical Rainfall Measuring Mission (TRMM) satellite, provide the first observations of total (intracloud and cloud-to-ground; IC and CG) lightning in TCs around the world (Cecil and Zipser, 1999; Cecil et al., 2002; Xu et al., 2017). Different from the orbiting satellites that view a fixed area over a short time, lightning imagers on board geostationary satellites launched in recent years have provided continuous sampling of total lightning with a higher detection efficiency (Goodman et al., 2013). These instruments include the Geostationary Lightning Mapper (GLM; Fierro et al., 2018; Duran et al., 2021; Ringhausen and Bitzer, 2021) onboard Geostationary Operational Environmental Satellite-16 (GOES-16) and Lightning Mapping Imagery (LMI; Hui et al., 2020; Zhang et al., 2020a) onboard Fengyun-4A (FY-4A), which will provide more useful information on total lightning in TCs and reestablish the relationship between lightning activity and TC intensification.

WWLLN data have been widely utilized in recent studies to observe lightning activity and deep convection in TCs (Pan et al., 2010; DeMaria et al., 2012; Pan et al., 2014; Zhang et al., 2015; Stevenson et al., 2016; Stevenson et al., 2018). The global lightning detection system is the most suitable system for detecting TC lightning, particularly for the landfall period during which storms move from the open sea to coastal regions and then to land. Ground-based lightning location networks, such as the Chinese National Lightning Detection Network, detect lightning over land at a higher detection efficiency (80%–90%; Xia et al., 2015). However, the detection range is limited to several hundred kilometers off the coast, and the detection efficiency decreases with increasing distance from lightning to the network. Since the WWLLN provides continuous lightning detection (in both longitude and latitude) in coastal areas, this study employs WWLLN data to study lightning distribution in TCs making landfall (including pre-landfall, landfall and post-landfall) in China. Comparisons between lightning observations from the WWLLN and FY-4A LMI in Super Typhoon Mangkhut (2018) indicated that the temporal and spatial evolution of lightning observed in these two systems are consistent (Zhang et al., 2020a).

Previous studies have found that the radial distribution of TC lightning shows an obvious pattern with two maxima in the inner core and outer rainbands and one minimum in the inner rainbands (Cecil et al., 2002; DeMaria et al., 2012; Stevenson et al., 2016). A positive correlation has been shown between lightning frequency and the maximum sustained wind speed of TCs (Price et al., 2009; Whittaker et al., 2015; Kong et al., 2021). The increase in lightning frequency may indicate the enhancement of TC intensity (Abarca et al., 2011; Pan et al., 2014; Wang et al., 2016). Stevenson et al. (2018) proposed that TCs are more likely to intensify 24 h after a burst of inner-core lightning if 1) the storm is stable or intensifying prior to the burst and 2) the burst has initiated downshear inside the radius of maximum wind. Additionally, the azimuthal distribution of lightning in mature hurricanes is consistent with TC convective and precipitation structures (Molinari et al., 1994; Molinari et al., 1999). Samsury and Orville (1994) found that during the pre-landfall and post-landfall periods of Hurricanes Hugo and Jerry (1989), the majority of lightning is located in the right quadrants in the outer convective rainbands. This maximum coincides with the highest reflectivity region observed by land-based radar. Xu et al. (2017) investigated the characteristics of TC lightning using 16-year global data from TRMM LIS. This relationship is found in the variation in lightning density and radar quantities (volume of 30 dBZ echoes in the mixed phase) in the outer rainbands. For landing TCs in China, lightning activities vary largely from

storm to storm (Zhang et al., 2012), suggesting that many factors, from large-scale environments to vortex dynamics, can influence the lightning distribution during TC landfall.

Other studies have examined the connection between lightning and environmental factors (i.e., storm motion and vertical wind shear) and investigated their influence on lightning asymmetry. Lightning maximum and strong convection are generally found in the front quadrant of TC motion, particularly the right-front quadrant, indicating the importance of frictional convergence in the boundary layer (Corbosiero and Molinari, 2003). However, vertical wind shear is a more dominant factor than storm motion in producing TC lightning asymmetry, similar to the asymmetry in TC convection (Corbosiero and Molinari, 2002) and precipitation (Cecil, 2007; Pei and Jiang, 2018). Lightning tends to occur primarily downshear left in the inner core and downshear right in the outer rainbands both in the Atlantic (Corbosiero and Molinari, 2002) and Pacific storms (Stevenson et al., 2016; Wang et al., 2018). Chan et al. (2004) examined the convective asymmetry for 4 TCs making landfall in South China and found that convection was strengthened a few hours prior to landfall. Enhanced convection first occurred on the western side in the mid-to lower troposphere and then rotated to the southward side in the upper troposphere by cyclonic flow and upward motion. TC vortex tilts downshear in response to environmental wind shear, resulting in the enhancement of deep convection in this quadrant (Houze, 2010).

While most of the abovementioned studies focused on TC lightning over the oceans, few studies have been performed on landing TCs. A quantitative description of some of the fundamental questions concerning lightning variability in landing TCs is needed. These fundamental questions include, but are not limited to, 1) Does every storm produce lightning during its landfall? Are lightning distributions in landing TCs different from those in TCs over water? 2) How do the lightning densities evolve prior to, during, and after landfall? 3) How do environmental and TC-specific factors affect the lightning distribution? The current study aims to document the characteristics of TC lightning during landfall in China and to examine the radial and asymmetry distributions as a function of TC intensity, landing location, and vertical wind shear. Answers to these questions can help to improve our basic understanding of lightning activity in TCs during landfall and possibly be utilized as guidance for the prediction of deep convection in TCs when they are approaching the coastline and finally making landfall.

2 DATA AND METHODS

2.1 Lightning Data

Lightning data used in this study are from WWLLN (http://wwlln.net). The WWLLN is a global ground-based lightning detection network operated by the University of Washington (Virts et al., 2013). WWLLN sensors receive very-low-frequency radio waves emitted by lightning, and the network locates lightning *via* a time-of-arrival technique with at least five sensors (Rodger et al., 2006). WWLLN primarily detects CG lightning, although it is also capable of detecting some IC lightning. Studies have suggested that the detection efficiency of WWLLN ranges from 10% over the continental United States (Abarca et al., 2010) to greater than 20% over the oceans (Rudlosky and Shea, 2013). Furthermore, for strokes with peak currents larger than 50 kA, the detection efficiency of the network is above 50% (Holzworth et al., 2019). Despite the low detection efficiency, WWLLN is capable of detecting almost all lightning-producing storms (Jacobson et al., 2006) and has expanded the detection range away from land to the open ocean.

The number of WWLLN stations has continued to grow since the network was set up in 2004. Currently, the network consists of over 80 stations worldwide (Holzworth et al., 2019). In addition, WWLLN began to save the integration of the electromagnetic field and accomplished algorithm improvement in April 2009 (Holzworth et al., 2019). All these factors have led to a higher and more stable detection efficiency since 2010 than it was before (Wang et al., 2018; Holzworth et al., 2021). Thus, we use WWLLN data from 2010 to 2020 to analyze the characteristics of lightning in landfalling TCs in China.

In this study, TC lightning is defined as lightning occurring within a radius of 500 km from the TC center. Lightning is segregated into three radial regions: the inner core (0–100 km), the inner rainbands (100–200 km), and the outer rainbands (200–500 km). The radial extents are close to the mean radii of the 3 TC regions revealed by Jiang et al. (2013) and are commonly used in studies analyzing TC lightning over the northwest Pacific (Zhang et al., 2015; Wang et al., 2018). Our large TC samples from 2010–2020 result in robust data of 1,302,625 WWLLN lightning strokes to investigate in this study. Lightning data are grouped into sets of 1-h periods called individual time periods (ITPs). Only ITPs with at least one lightning stroke are analyzed, which resulted in a total of 3293 ITP samples to study.

2.2 TC Best-Track Data

TC best-track data are obtained from the China Meteorological Administration best-track dataset. The dataset gives the location and intensity of TCs every 6 h (sometimes 3 h) at synoptic times (0000, 0600, 1200, and 1800 UTC). The best-track data are linearly interpolated to hourly data to estimate the distance of lightning to the storm center. In this study, TC intensities are classified into two categories based on the maximum wind speed at the time when lightning occurs: 1) weak TC (WTC) with sustained maximum wind speed $<32.7\ m\ s^{-1}$, including tropical depression (TD, $10.8–17.1\ m\ s^{-1}$), tropical storm (TS, $17.2–24.4\ m\ s^{-1}$), and severe tropical storm (STS, $24.5–32.6\ m\ s^{-1}$); 2) strong TC (STC) with sustained maximum wind speed $\geq 32.7\ m\ s^{-1}$, including typhoon (TY, $32.7–41.4\ m\ s^{-1}$), severe typhoon (STY, $41.5–50.9\ m\ s^{-1}$) and super typhoon (SuperTY, $\geq 51\ m\ s^{-1}$).

2.3 Environmental Variables

The vertical wind shear is quantified by using pressure level data, i.e., the U-component and V-component of wind form the European Centre for Medium-Range Weather Forecasts (ECMWF) reanalysis (ERA5, https://cds.climate.copernicus.eu/)

TABLE 1 | Samples of TCs at different intensity levels by the time of landfall in mainland China from 2010 to 2020.

Year	TS (17.2–24.4 m s^{-1})	STS (24.5–32.6 m s^{-1})	TY (32.7–41.4 m s^{-1})	STY (41.5–50.9 m s^{-1})	SuperTY (≥51 m s^{-1})	Total
2010	2	0	5	0	0	7
2011	4	2	2	0	0	8
2012	1	1	1	2	0	5
2013	2	3	1	3	0	9
2014	2	2	0	1	1	6
2015	0	3	1	0	1	5
2016	2	1	4	0	1	8
2017	3	3	1	1	0	8
2018	7	2	1	1	0	11
2019	5	0	1	1	0	7
2020	1	1	2	1	0	5
Total	29 (37%)	18 (23%)	19 (24%)	10 (12%)	3 (4%)	79 (100%)

TD, tropical depression; TS, tropical storm; STS, severe tropical storm; TY, typhoon; STY, severe typhoon; SuperTY, super typhoon.

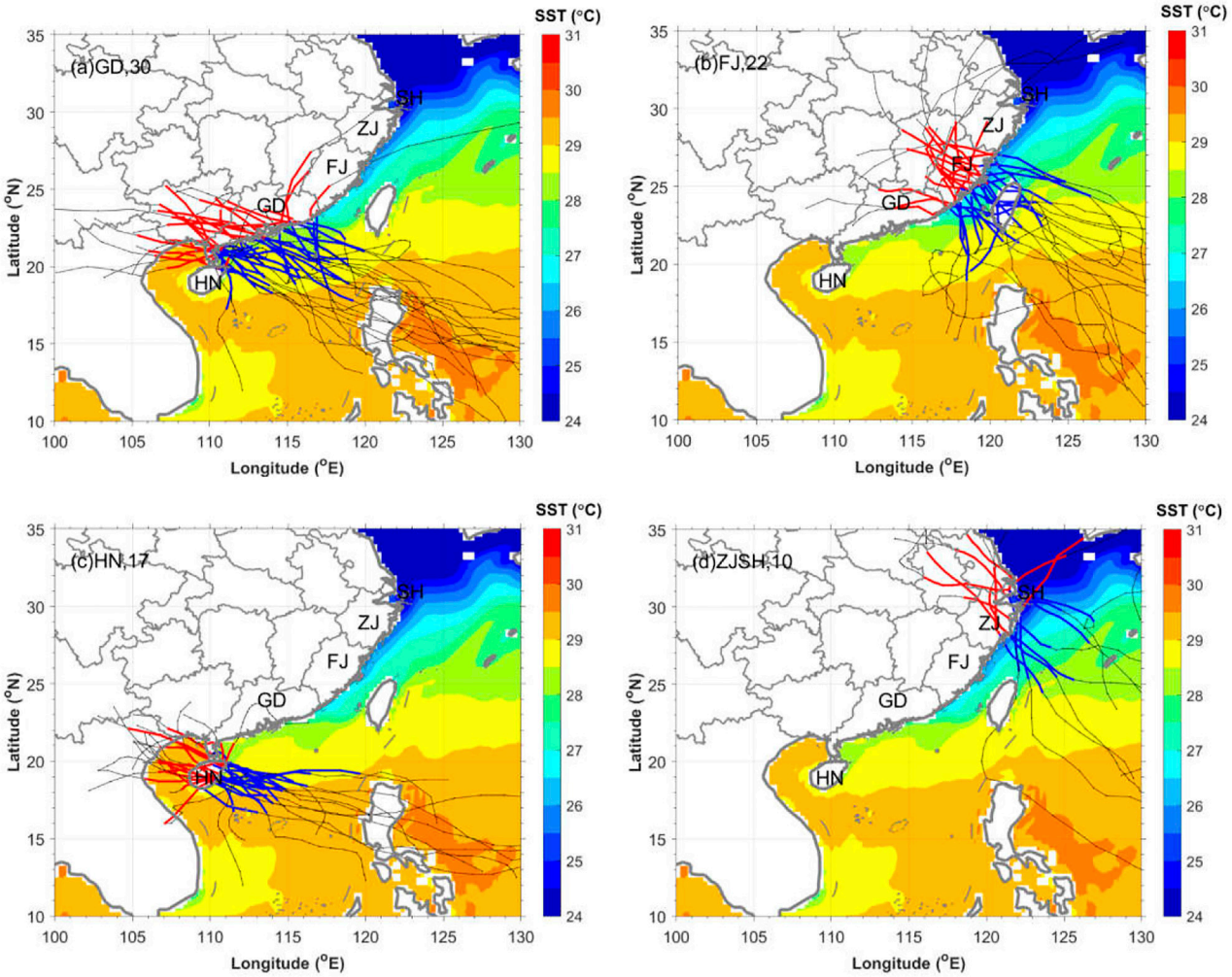

FIGURE 1 | Best tracks and samples of tropical cyclones that made landfall in different regions over China from 2010 to 2020 overlaid with SST. **(A)** Guangdong (GD), **(B)** Fujian (FJ), **(C)** Hainan (HN), and **(D)** Zhejiang and Shanghai (ZJSH). The blue lines indicate the tracks 24 h prior to landfall, the red lines indicate the tracks 24 h after landfall, and the black lines indicate the tracks beyond the 48-h landfall period. The numbers in the figure indicate the landfall samples in that region. SST data are the mean value for the TC season (June to October) in 1989–2019 from the ERA5 database.

dataset. The dataset is available hourly at 0.25° resolution in latitude and longitude. Deep-layer vertical wind shear is calculated between 850 and 200 hPa by averaging horizontal winds over a radius of 500 km from the storm center. This method was also adopted by Corbosiero and Molinari (2002) and DeMaria et al. (2012).

2.4 Methodology

2.4.1 Sample Selection and Definitions

The cases analyzed in this study are confined to TCs at the strength of tropical storms or greater by the time of landfall. TCs that landed north of 35°N are excluded to avoid the extratropical cyclone. The landfall period is confined to 48 h from 24 h prior to landfall to 24 h after landfall. TCs that dissipated within 24 h of landfall are also included.

TC landing locations are determined based on the following standards. ① According to the provinces on mainland China where TCs made landfall, the landfall locations are grouped into four categories: Guangdong (GD), Hainan (HN), Fujian (FJ), and Zhejiang and Shanghai (ZJSH). ② If a storm first made landfall over Taiwan and arrived at mainland China (e.g., FJ) for its second landfall, the landfall location is recorded as the mainland location (FJ). ③ For a TC that made landfall more than one time, if the time interval between the second landing and the first landing is <6 h, the first landfall is considered. If the landfall interval is ≥6 h, the second landfall is taken as a new landfall sample. Since the landfall time is not exactly synoptic time given by the best-track dataset, the nearest synoptic time (0000, 0600, 1200, and 1800 UTC) is used as the landfall time (Yu et al., 2017). Based on the above criteria, a total of 79 landfalls from 74 TCs are selected in 2010–2020 over mainland China, including 29 TSs, 18 STSs, 19 TYs, 10 STYs, and 3 SuperTYs (**Table 1**). The 79 landfalls are distributed over the provinces of GD with 30 landfalls, FJ with 22 landfalls, HN with 17 landfalls, and ZJSH with 10 landfalls (**Figure 1**).

2.4.2 Asymmetry Analysis

In analyzing the asymmetry distributions, lightning data are rotated to the shear vector and put into shear-relative coordinates. Each lightning is represented by the distance from its location to the storm center and its rotation angle with respect to the shear vector. Lightning densities are grouped into four quadrants: downshear-right (DR), downshear-left (DL), upshear-right (UR) and upshear-left (UL). The magnitude of the asymmetry in lightning density is calculated following Cecil (2007) and Xu et al. (2014). First, with a radius step of 100 km, the lightning density of five annular regions in each quadrant is calculated. Then, the average value of the five annular regions is the average lightning density for that quadrant. Last, the asymmetry magnitude is defined as the ratio of the averaged lightning density in the favored quadrants to that in the unflavored quadrants relative to shear. To investigate the impact of shear on lightning asymmetry, shear magnitudes are grouped into three categories: low shear (<5 m s^{-1}), moderate shear (5–10 m s^{-1}), and high shear (>10 m s^{-1}).

3 CHARACTERISTICS OF TC LIGHTNING RATE

3.1 Overall and The Extreme

Each storm in our cases produces lightning during its 48-h landfall period. The WWLLN detected lightning activity in all TCs that made landfall in 2010–2020, with the average and median lightning rates of 364 and 174 stroke h^{-1}, respectively. Tropical Storm Haitang (2017) produced the highest amount of lightning, with 71,055 strokes in 48 h landing in Fujian. In contrast, Severe Tropical Storm Ampil (2018) has the lowest lightning count, with only 6 strokes during its 48-h landfall in Shanghai. Among all the detected lightning, 56% of lightning occurred before landfall and 44% after landfall (**Table 2**); 6.2% occurred in the inner core, 9.6% in the inner rainbands, and 84.2% in the outer rainbands; 27.9% occurred during the intensification stages (ΔVmax>0), 49.9% in the weakening stages (ΔVmax<0), and 22.2% in the stable stages. **Table 3** shows the top ten storms with the highest lightning count during landfall. All these active-lightning storms made landfall between June and September. Five of the storms (Fanapi, Matmo, Nepartak, Nida, and Kalmaegi) made landfall at intensity levels ≥TY, and the others (Haitang, Bailu, Bebinca, Kujira, and Doksuri) made landfall at intensity levels of TS and STS.

The extreme hourly lightning rate in the inner core is 3,154 str h^{-1} generated by Tropical Storm Cimaron (2013). It occurred at 0100 UTC on 18 July 2013, 10 h before Typhoon Cimaron made landfall in Fujian (**Figure 2A**). The center of Cimaron was located in the north of the South China Sea and off the coast of southeastern Fujian, at approximately 21.9°N and 118.1°E. The maximum sustained winds were approximately 23 m s^{-1}, making the storm a TS. Cimaron was moving almost due north. TC lightning was mainly concentrated in the inner-core region at this hour on the right and front right of the storm motion. The majority of the extreme inner-core cases occur south of 23°N prior to landfall, indicating that a large inner-core lightning rate tends to occur in low-latitude oceanic regions with high sea surface temperatures (SSTs).

The extreme hourly lightning rate in the outer rainbands is 4,426 str h^{-1}, produced by Severe Typhoon Matmo (2014). It occurred 7 h after Matmo's landfall in Fujian at 1200 UTC on 23 July 2014 (**Figure 2B**). The maximum wind speed was 25 m s^{-1}, and the minimum sea level pressure was 988 hPa (STS intensity level). The eyewall structure was not clear, and TC lightning displayed strong asymmetry. The strong convections were mainly located in a long and narrow rainband to the south of the storm center. The convective elements in the outer rainbands developed arc-shaped lines observed by coastal radars, indicating that the storm was reacting to land surfaces. Previous studies revealed that the electrification mechanism in the outer rainbands is markedly different from that in the eyewall but more likely similar to that of ordinary cumulonimbus (Williams, 1988; Houze, 2010). The high lightning rate in the rainband region is comparable to lightning activity in mesoscale convection systems on land (Liu et al., 2021).

TABLE 2 | The statistics of lightning strokes at different periods, regions and stages during TC landfall.

Period		Region			Stage			Lightning count (48 h)	
Prior to landfall	**After landfall**	**Inner rainbands**	**Inner core**	**Outer rainbands**	**Intensifying**	**Stable**	**Weakening**	**Maximum**	**Minimum**
$t_{-24\sim0}$	$t_{0\sim+24}$	100–200 km	0–100 km	200–500 km	ΔVmax>0	ΔVmax=0	ΔVmax<0	strokes	strokes
56%	44%	9.6%	6.2%	84.2%	27.9%	22.2%	49.9%	71,055	6

TABLE 3 | The top ten storms in 2010–2020 with the largest lightning count during the 48-h landfall period. V_{max} and intensity are the maximum wind speed (m s^{-1}) and its intensity level during the 48-h landfall period. Lightning count is the number of lightning strokes in the whole TC region (0–500 km).

Rant	TC	Year	Month	Landfall	V_{max} (m s^{-1})	Intensity	Landfall hours	Lightning count	Mean TC lightning rate (str h^{-1})
1	Haitang	2017	Jul	FJ	24	TS	48	71,055	1480
2	Fanapi	2010	Sep	FJ	45	STY	48	67,763	1412
3	Bailu	2019	Aug	FJ	30	STS	48	53,928	1124
4	Matmo	2014	Jul	FJ	42	STY	48	52,132	1086
5	Nepartak	2016	Jul	FJ	38	TY	42	47,200	1124
6	Nida	2016	Aug	GD	36	TY	48	43,609	909
7	Bebinca	2018	Aug	GD	28	STS	48	43,094	898
8	Kalmaegi	2014	Sep	HN	42	STY	48	42,506	886
9	Kujira	2015	Jun	HN	25	STS	48	37,970	791
10	Doksuri	2012	Jun	GD	24	TS	36	31,848	885

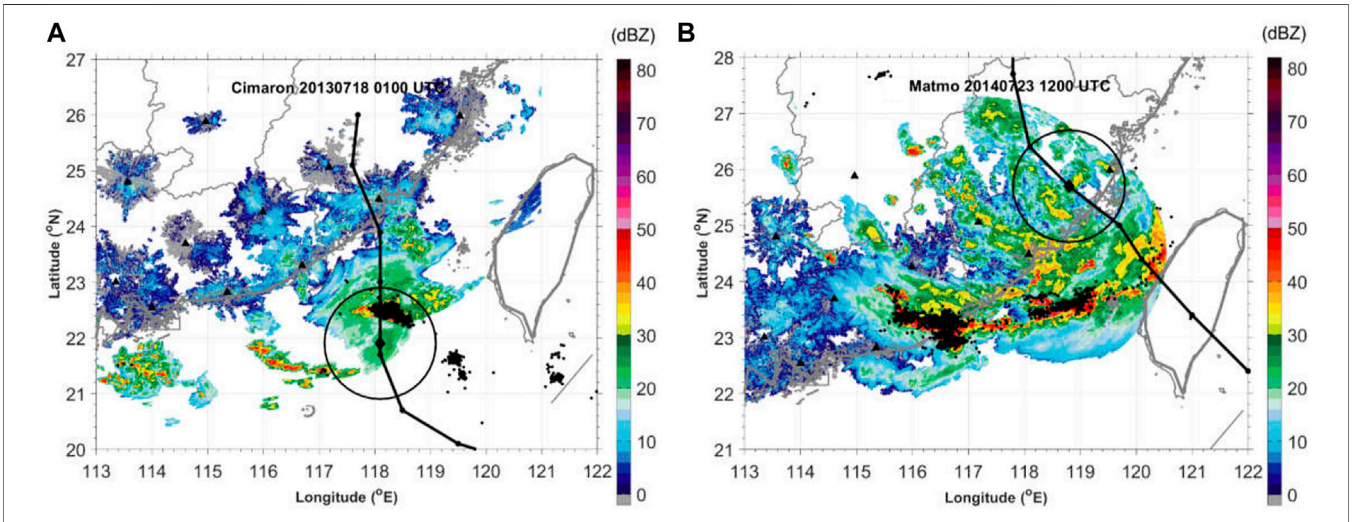

FIGURE 2 | Overlay of lightning activity and radar composite reflectivity at the hours producing the maximum lightning rates in **(A)** the inner core for Tropical Storm Cimaron (2013) and **(B)** the outer rainbands for Severe Typhoon Matmo (2014). The black dots denote WWLLN strokes. The black triangles represent the costal radar stations. The black circle indicates the 100-km radius from the storm center.

3.2 PDF of Lightning Rates

The probability density function (PDF) of lightning rates represents the basic characteristics of lightning activity. **Figure 3** shows the PDF distributions of lightning rates for all ITPs calculated within 500 km of the storm center. Lightning rates are shown on a dB scale or $10\times\log_{10}$ (lightning rates). The lightning rates of landing TCs are between 1 and 4,447 str h^{-1}. The mode is approximately 400 str h^{-1} for all the samples, and lightning rates most frequently appear between 250 and 600 str h^{-1} (**Figure 3A**). The occurrence frequency for lightning rates higher than 100 str h^{-1} is relatively higher in pre-landfall samples than post-landfall samples, indicating that lightning is more active when the storm center is over water.

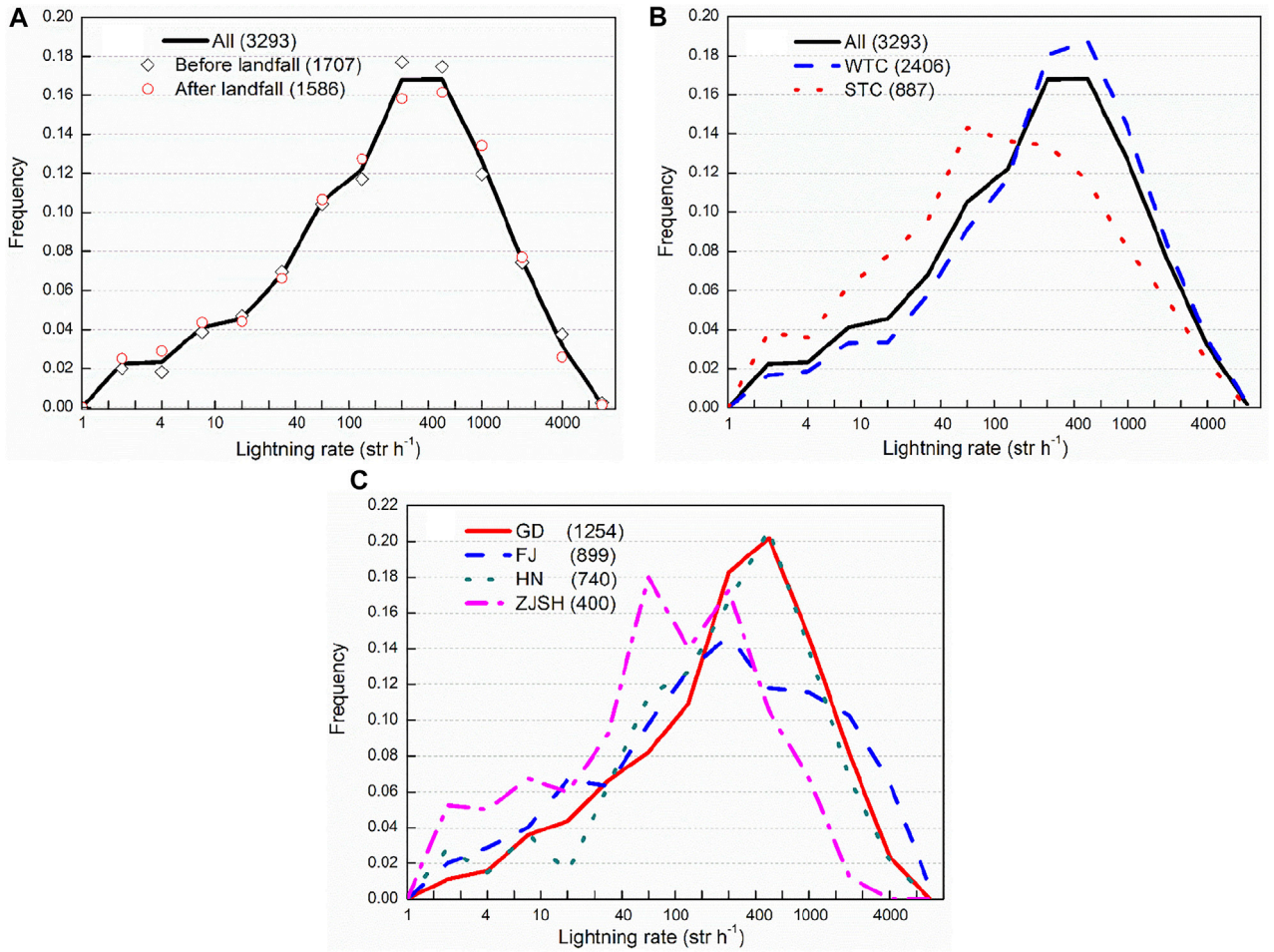

FIGURE 3 | Probability density functions of lightning rates within 500 km of the storm center for **(A)** before and after landfall groups, **(B)** weak and strong groups, and **(C)** landing location groups. The number in parentheses indicates the samples.

For the PDF distribution of different intensity categories (**Figure 3B**), the lightning rates shift toward lower values as the storm intensities increase. For WTC, the highest probability is approximately 18% for a lightning rate of 400 str h^{-1}, while for STC, the highest probability drops to approximately 14% for 63 str h^{-1}. When the lightning rate exceeds 158 str h^{-1}, the PDF probability in WTC is higher than that in STC, indicating that weaker TCs would have higher probabilities of larger lightning rates during landfall. The 75% (50%) percentiles of the lightning rate are 530 (211) str h^{-1} for WTC and 288 (83) str h^{-1} for STC. Previous studies based on WWLLN data have found that lightning tends to occur in weak storms and that samples of lightning occurrence in WTCs are larger than those in STCs when TCs are over water (Abarca et al., 2011; Zhang et al., 2015; Wang et al., 2018; Lin and Chou, 2020). Our study confirms that this relationship also exists during TC landfall. Based on infrared satellite observations, Zhang et al. (2020b) revealed that the large contribution of lightning in WTCs is due to the high occurrence of deep convection (IR<220 K) in these weak storms during their landfall.

In the distribution of PDFs for different landing locations, the frequency and amplitude of the PDF show some differences (**Figure 3C**). TCs landing in Guangdong and Hainan have the largest peak lightning rates and the narrowest distributions, and the PDF distribution is similar to the overall PDFs. However, TCs that made landfall in Fujian show a reduced peak lightning rate but with a wider distribution. In **Table 3**, we find that TCs landing in Fujian could also produce high lightning rates at certain hours, which leads to the wide PDF distribution skewed toward higher rates. The PDF distribution of the lightning rate in Zhejiang and Shanghai is bimodal, with one peak at approximately 250 str h^{-1} and a second peak near 60 str h^{-1}. Note that when the lightning rate is greater than 400 str h^{-1}, the distribution frequency decreases rapidly for ZJSH. One possible reason is the lower SST in coastal regions that are north in latitude (>23.5°N). Previous studies (e.g., Stevenson et al., 2016; Xu et al., 2017) found that TC lightning tends to occur in areas with warmer SSTs. Lower SSTs inhibit environments that support strong convection and active lightning activity. **Figure 3** indicates that both TC intensity and landfall

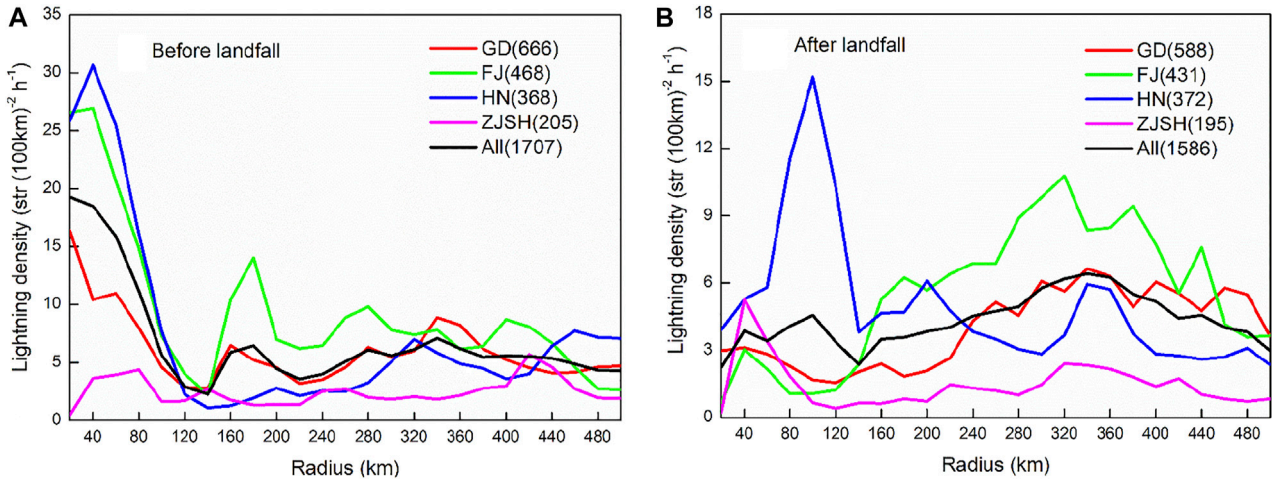

FIGURE 4 | Radial distribution of lightning density (str (100 km)$^{-2}$ h^{-1}) in TCs at different landing locations **(A)** 24 h before and **(B)** 24 h after landfall.

locations are important factors that affect lightning rates in landing TCs.

4 CHARACTERISTICS OF TC LIGHTNING DISTRIBUTION

4.1 Radial Distribution

It is important to show how the radial distributions of lightning vary according to landing stages, locations and TC intensities. The mean lightning density is computed using 20-km bins from the storm center to a radius of 500 km and then averaged in each azimuthal bin. **Figure 4** shows the radial distribution of lightning density in TCs landing at different locations 24 h before (t_{-24}~t_0) and after (t_0~t_{+24}) landfall. In general, for all samples, the peak lightning density is located within 40 km from the storm center and is approximately 22 str (100 km)$^{-2}$ h^{-1} prior to landfall (**Figure 4A**). The variability in the radial distribution is large from geographic location to location. The mean lightning densities vary between 5 and 30 str (100 km)$^{-2}$ h^{-1} within the inner core before landfall, possibly because of the different environments in which the eyewall was embedded. The lightning density reaches the minimum at a radius of 120 km (inner rainbands) and then increases again in the outer rainbands. The radial structure of TC lightning before landfall corresponds well to the lightning distribution in mature hurricanes (DeMaria et al., 2012).

After TC made landfall, the averaged lightning density drops to approximately 6 str (100 km)$^{-2}$ h$^{-1,}$ and the maximum shifts to the outer rainbands approximately 350 km from the center (**Figure 4B**). Therefore, the peak lightning density decreases significantly during landfall and shifts outward from the eyewall to the outer rainbands, which is consistent with Zhang

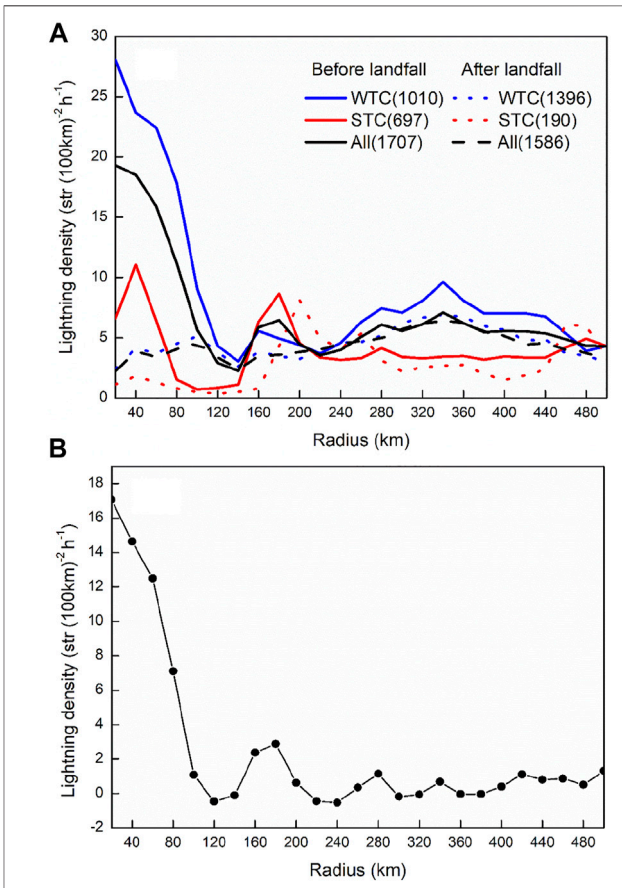

FIGURE 5 | Radial distribution of **(A)** lightning density (str (100 km)$^{-2}$ h^{-1}) for weak (TD\TS\STS) and strong (TY/STY/SuperTY) TCs 24 h before and after landfall, and **(B)** lightning density before landfall minus after landfall.

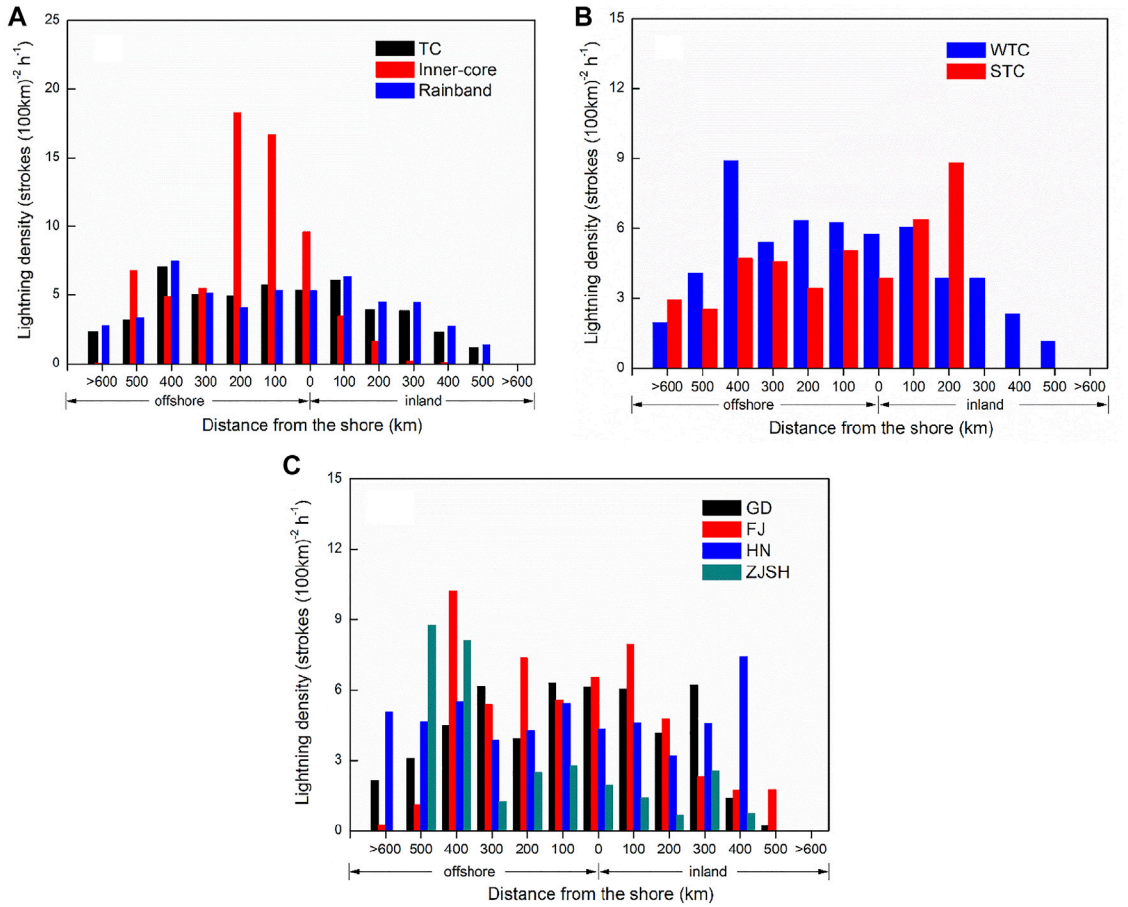

FIGURE 6 | Mean TC lightning density (strokes (100 km)$^{-2}$ h^{-1}) as a function of distance from the shoreline for categories of **(A)** TC regions, **(B)** TC intensities (weak TC and strong TC), and **(C)** landing locations.

et al. (2012). This is due to eyewall collapse and the enhanced surface frictional convergence in the outer rainbands during the landfall period. Note that there is an exception in the outward movement of lightning density. For TCs making landfall in HN, there is still a peak of lightning density in the inner-core region after landfall. This distribution is consistent with the radial structure of precipitation of TCs landing in HN (Yu et al., 2017). The comparison between **Figures 4A,B** obviously reflects the impact of landfall on lightning activity for TCs in different regions over China.

Figure 5 shows the radial distribution of lightning density for different TC intensity categories before and after landfall. For weak storms (i.e., TS category), the averaged lightning density within the inner core prior to landfall is much higher than that after landfall. Lightning densities larger than 25 str (100 km)$^{-2}$ h^{-1} are found within 40 km of the storm center and decrease to 5–10 str (100 km)$^{-2}$ h^{-1} at 200–440 km in weak TCs before landfall (**Figure 5A**). For strong storms (i.e., TY category), lightning densities in both the inner core and the outer rainbands are lower than those of weak storms. Overall, the averaged lightning densities in all radii decreased after landfall, with the largest reduction in the inner-core region (**Figure 5B**). In addition, after landfall, the difference in lightning density between STC and WTC decreases sharply. Lightning density in weak storms decreases more sharply with radius compared to strong storms during the 48-h landfall. Total lightning observations from LIS and GLM revealed that the dominant type of lightning (IC or CG) and rain regime (oceanic or continental) may change from the outer rainbands to the inner core (Cecil et al., 2002; Yokoyama and Takayabu, 2008; Fierro et al., 2018). The high lightning rate within the inner core may be related to the increased ratio of IC to CG lightning in that region.

4.2 Lightning Density With Distance From the Shore

Due to the weakening of TC intensity and the collapse of its structure, it is believed that lightning activity tends to weaken as landfall approaches as well as after making landfall. However, interactions between TC remnants and outer rainbands with land may also produce strong lightning much farther inland from the coast (Samsury and Orville, 1994; Zhang et al., 2012). Here, we investigate the mean TC lightning density as a function of distance from the shore (**Figure 6**). The distance is defined as

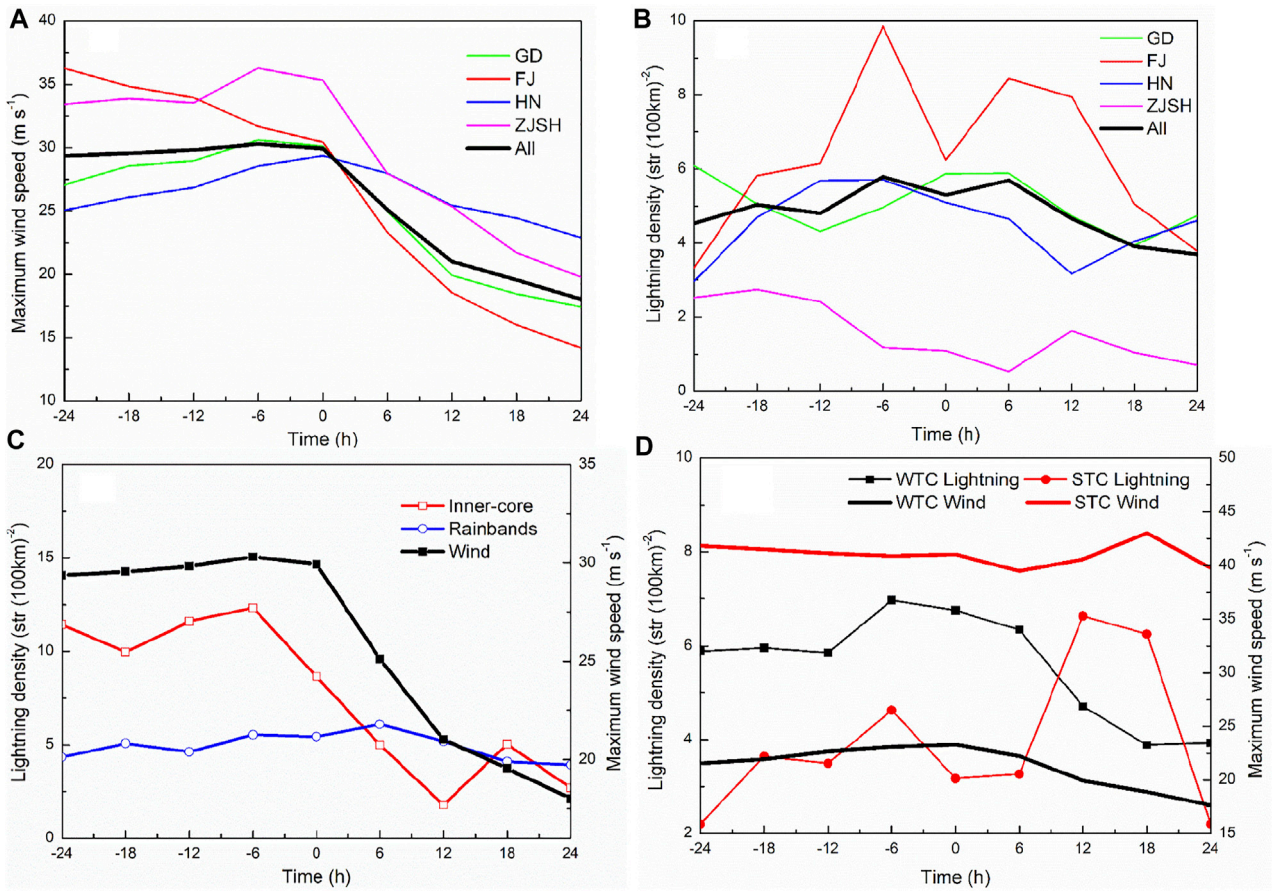

FIGURE 7 | Evolution of the mean maximum wind speed and lightning density (str (100 km)$^{-2}$) as a function of **(A,B)** landing locations, **(C)** TC regions, and **(D)** TC intensities at 6-h intervals from 24 h prior to and 24 h after landfall.

the closest distance from the TC center to the coastline. For lightning in TC and the outer rainband, the maximum density can be found when the TC center is located approximately 400 km offshore from the shoreline (**Figure 6A**). Lightning density gradually decreases as the storm moves inland and then remains constant at lower values in coastal areas 0–300 km from the shoreline. It is worth noting that the largest inner-core lightning density occurs before landfall when the TC center is located 100–200 km away from the coastline. This implies that when TCs are about to make landfall, strong lightning and convection could occur in the inner core, which may cause TCs to strengthen again in coastal areas. The possible reason is the re-strengthen of some typhoons when locate about 100–200 km away from the coastline, causing intense lightning activity within the inner-core region. Typhoon Hato (2017) is an example. The inner-core lightning tends to weaken faster than the outer rainbands with inland distance due to the collapse of the eyewall structure.

Weak storms produce the largest lightning density when the centers are located approximately 400 km onshore during pre-landfall. The lightning densities of the WTC gradually decrease after landfall. On the other hand, the lightning density of strong storms increases after landfall, and the largest value is found when the TC center moves 200 km inland (**Figure 6B**). For TCs landing in Guangdong and Fujian, lightning is mainly confined within 300 km from the shoreline in both inland and coastal areas (**Figure 6C**). TCs landing in Zhejiang and Shanghai produce the most lightning when their centers are 400–500 km onshore. The subsequent rapid decrease is likely related to the farther north landing locations and the lower SST in that coastal area. For TCs landing on Hainan Island, there is a weaker dependence of TC lightning on the distance from the shoreline.

Figure 7 shows the evolution of the hourly lightning density and maximum wind speed during the 48-h landfall period. From 24 to 6 h (t_{-24}~t_{-6}) prior to landfall, the mean maximum wind speeds increase for TCs making landfall in GD, HN, and ZJSH. However, the wind speeds decrease for TCs making landfall in FJ, which is probably due to the weakening effect of Taiwan Island on TC intensity. After the storm makes landfall (t_0~t_{24}), all the maximum wind speeds decrease rapidly (**Figure 7A**). **Figures 7B,C** show the evolution of the mean lightning density in the whole TC region (0–500 km), the inner core and the outer rainbands. The variations of lightning density in whole TC (black line in **Figure 7B**) and outer rainbands (blue line in

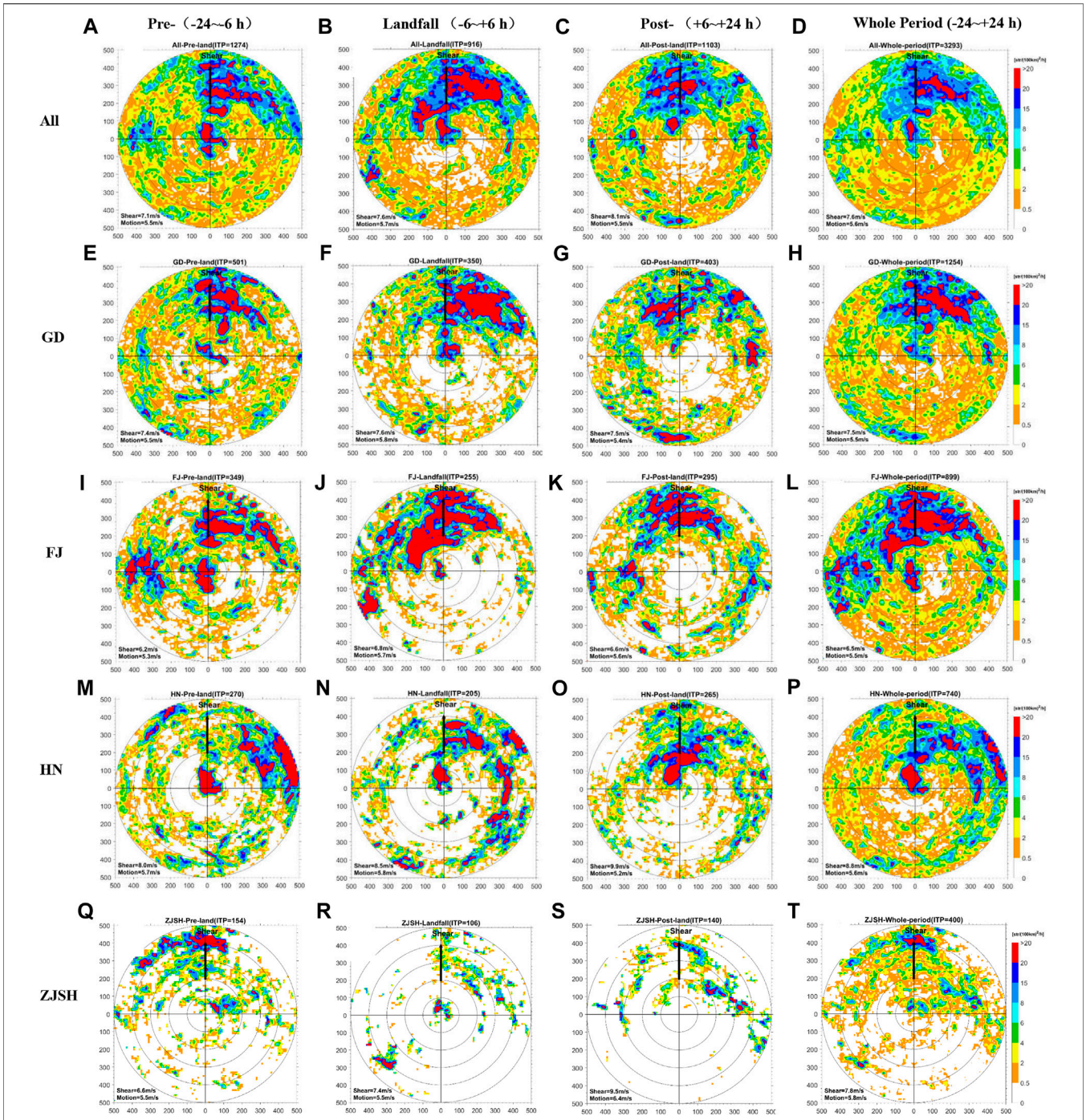

FIGURE 8 | Shear-related lightning density (str (100 km)$^{-2}$ h^{-1}) as a function of landing location for pre-landfall (-24~-6 h), landfall (-6~+6 h), post-landfall (+6~+24 h), and the whole period (-24~+24 h). **(A–D)** all ITPs, **(E–H)** Guangdong, **(I–L)** Fujian, **(M–P)** Hainan, **(Q–T)** Zhejiang and Shanghai.

Figure 7C) is not large, which is not consistent with the trend of wind speeds during the landfall period. In contrast, lightning density in the inner-core region is positively related to TC wind speed (**Figure 7C**). At 6 h prior to landfall, the averaged maximum wind speed and the inner-core lightning density both reach their peak values. In the following 30 h (t_{-6}~t_{24}), the averaged maximum wind speed decreases from 30 m s^{-1} to approximately 18 m s^{-1}, with a decrease rate of 40%. Consequently, the inner-core lightning densities decrease with the weakening of wind speed during this period. Furthermore, the decrease rate of inner-core lightning density is much higher than that of the outer rainbands, indicating that lightning activity within the inner core is more affected by TC intensity. It is interesting to note that during the period of 6–18 h after landfall

(t_6~t_{18}), lightning densities in strong TCs increase with the rise of averaged maximum wind speeds, with the peak of lightning approximately 6 h prior to the peak of wind speed (**Figure 7D**).

5 ASYMMETRY DISTRIBUTION OF TC LIGHTNING

5.1 Asymmetry Distribution as a Function of Landing Location

Figure 8 shows the lightning distribution as a function of landing locations and periods, i.e., pre-landfall (−24~−6 h), landfall (−6~+6 h), post-landfall (+6~+24 h), and whole period (−24~+24 h). In general, all the regions show clear lightning and convection asymmetries, with lightning maxima in the downshear (DL and DR) quadrants prior to, during, and after landfall. This indicates that vertical wind shear plays a major role in the asymmetric distribution of convection during the 48-h landfall period, and the effect of motion is secondary to that of shear. Corbosiero and Molinari (2002) and Stevenson et al. (2016) found that the downshear-favored lightning maximum is obvious even though the storm is moving in the opposite direction of the wind shear. This is also evident in this study for TCs making landfall in ZJSH (**Figures 8Q–T**). Although the averaged angle between the shear and motion vectors is larger than 130°during pre-landfall in ZJSH, the convection is still concentrated in the downshear quadrants. However, it is worth noting that there is a difference in lightning asymmetry between the inner core and outer rainbands. The inner-core lightning tends to distribute in the DL quadrant, while the outer-rainband lightning is distributed in the downshear to DR quadrants (**Figures 8D,H,L,P,T**). These structural changes in different TC regions are consistent with Stevenson et al. (2016) and Corbosiero and Molinari (2002).

In addition to vertical wind shear, the spatial distribution of lightning asymmetry is also related to the landing locations. TCs landing in ZJSH produce the least lightning and a much smaller area of high lightning density than TCs landing in other regions (**Figures 8Q–T**). In contrast to other TCs in which lightning is distributed throughout the whole outer rainbands, lightning in ZJSH TCs is mainly concentrated on the downshear side at 400–500 km. This is due to the higher latitude (~30°N) of the ZJSH regions and the lower SST in their adjacent waters. We also noted that storms landing at ZJSH have higher maximum wind speeds (**Figure 7A**), and this could be another reason for the low lightning occurrence at ZJSH. The climatological distribution of lightning over the northwest Pacific suggests that the TC lightning maximum occurs in the northern part of the South China Sea over warmer SSTs (28–30°C) (see **Figure 5** in Zhang et al., 2020b). In the adjacent sea of ZJSH, the mean SST in the TC season (June-October) is approximately 26°C (**Figure 1D**). This value is much lower than the necessary thermodynamic threshold (SST of 26°C) supporting TC deep convection indicated by Gray (1968). An environment of SST between 28°C and 30°C is favored for stronger convection and higher lightning counts, which is referred to as the "sweet spot" for TC lightning (Stevenson et al., 2016).

Figure 8 also shows the changes in lightning asymmetry in different stages of the landfall period. As TCs move from waters (−24~−6 h; **Figures 8A,E,I,M,Q**) to the coastline (−6~+6 h; **Figures 8B,F,J,N,R**) and finally make landfall (+6~+24 h; **Figures 8C,G,K,O,S**), the distributions of inner-core lightning experience some significant changes. The inner-core lightning is the strongest when TCs are over the open water, with the maximum concentrated in the downshear quadrants. When TCs approach the coast and make landfall, the area of maximum lightning within the inner core is decreased, and its asymmetry distribution is enhanced, which is mainly confined to DL quadrants. Meanwhile, we also noticed that active inner-core lightning is also observed in the upshear quadrant during pre-landfall. Stevenson et al. (2016) found that in some fast-moving TCs in the eastern North Pacific with opposite motion and shear vectors, lightning peaked upshear (i.e., downmotion) instead of downshear sides. Inner-core lightning maximum and convective bursts on the upshear side were also observed during the intensification of Tropical Storm Gabrielle (2001; Molinari et al., 2006) and Hurricane Earl (2010; Stevenson et al., 2014; Susca-Lopata et al., 2015). Deep convection initiated left of shear and then rotated into upshear regions. This convective rotation contributed to TC intensification by making the vortex more aligned and symmetric.

For the outer-rainband lightning, the downshear quadrants dominate its distribution for the whole landfall period. When TC approaches the coast and makes landfall (−6~+6 h), lightning densities in the 200–400 km outer rainbands gradually increase (except for TCs in ZJSH) on the downshear sides (**Figures 8B,F,J,N**). This is due to the strengthening of the frictional convergence between the rainbands and land surface, which plays an important role in the enhancement of convection for landing TCs. During the post-landfall period (+6~+24 h), lightning in the outer rainbands decreases as TCs gradually weaken over land.

5.2 Asymmetry Distribution as a Function of TC Intensity

Lightning asymmetries as a function of TC intensity for different landing periods are shown in **Figure 9**. The ITPs are grouped into WTC cases (<32.7 m/s, ITP=2,406) and STC cases (≥32.7 m/s, ITP=887). In general, the maximum lightning is generally downshear for all cases. As the storms move onshore (**Figures 9A,B**), approach the coast (**Figures 9C,D**), and finally make landfall (**Figures 9E,F**), lightning asymmetries shift slightly cyclonically to the left. Chan et al. (2004) also observed intense convection rotated counterclockwise to the left prior to and during landfall of Typhoons Sam (1999) and York (1999). Furthermore, **Figure 9** indicates that WTCs show stronger lightning densities and larger maximum density areas than STCs. When TCs intensify into typhoons, severe typhoons and super typhoons, the area of high lightning density decreases markedly, especially within the inner-core region (**Figures 9B,D,F,H**). The reason weak storms produce more lightning activity during landfall needs further study.

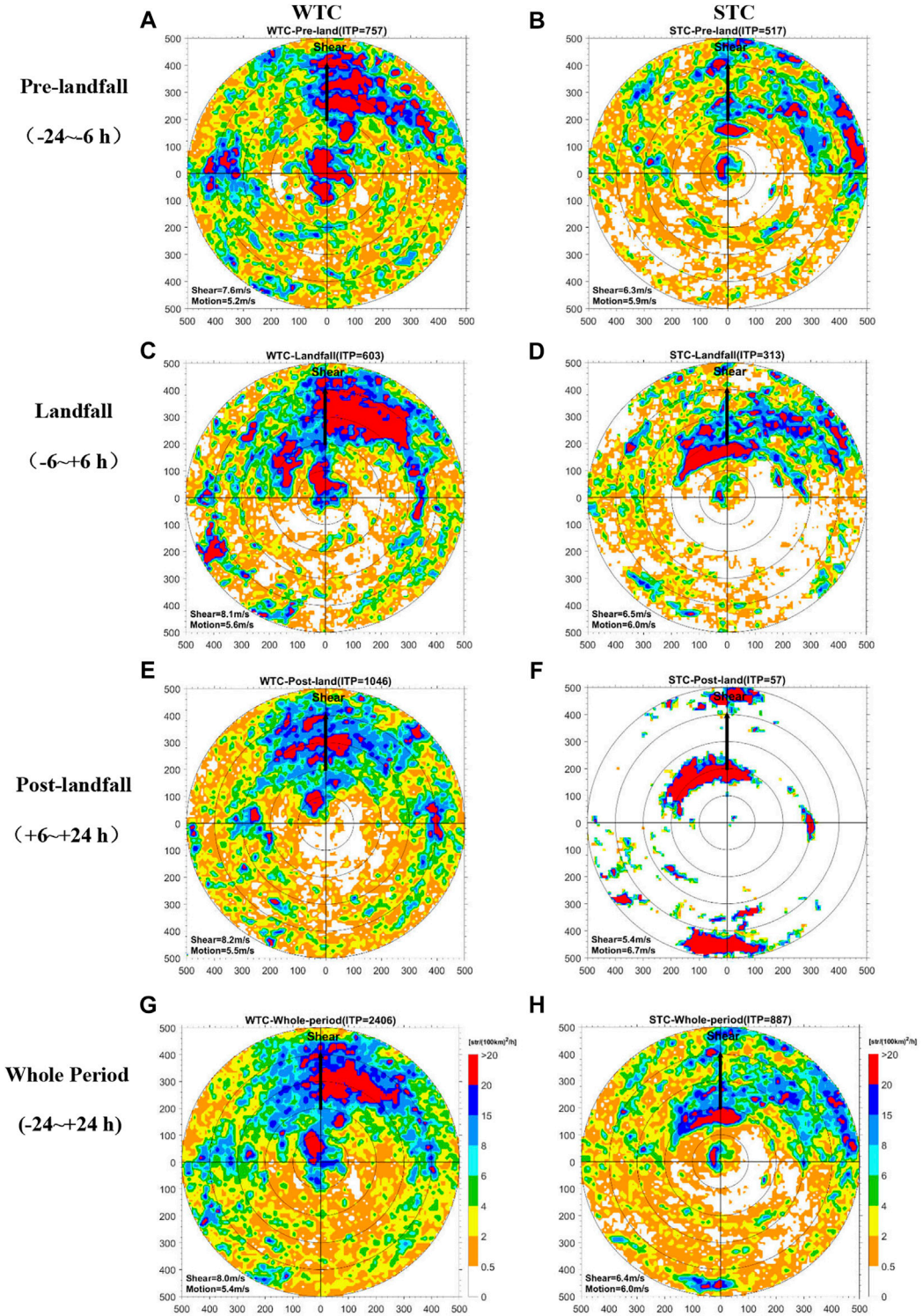

FIGURE 9 | Shear-related lightning density (str (100 km)$^{-2}$ h^{-1}) as a function of storm intensity for **(A,B)** pre-landfall (–24~–6 h), **(C,D)** landfall (-6~+6 h), **(E,F)** post-landfall (+6~+24 h), and **(G,H)** the whole period (–24~+24 h). **(A,C,E,G)** Weak TCs, **(B,D,F,H)** Strong TCs.

It is notable that strong axisymmetric lightning within the inner core in STCs during pre-landfall is observed (**Figure 9B**), which indicates that inner-core deep convections in STCs are more organized than those in WTCs. The difference in deep convection asymmetry in the inner core between the STC and WTC might be due to, on the one hand, the strength of the

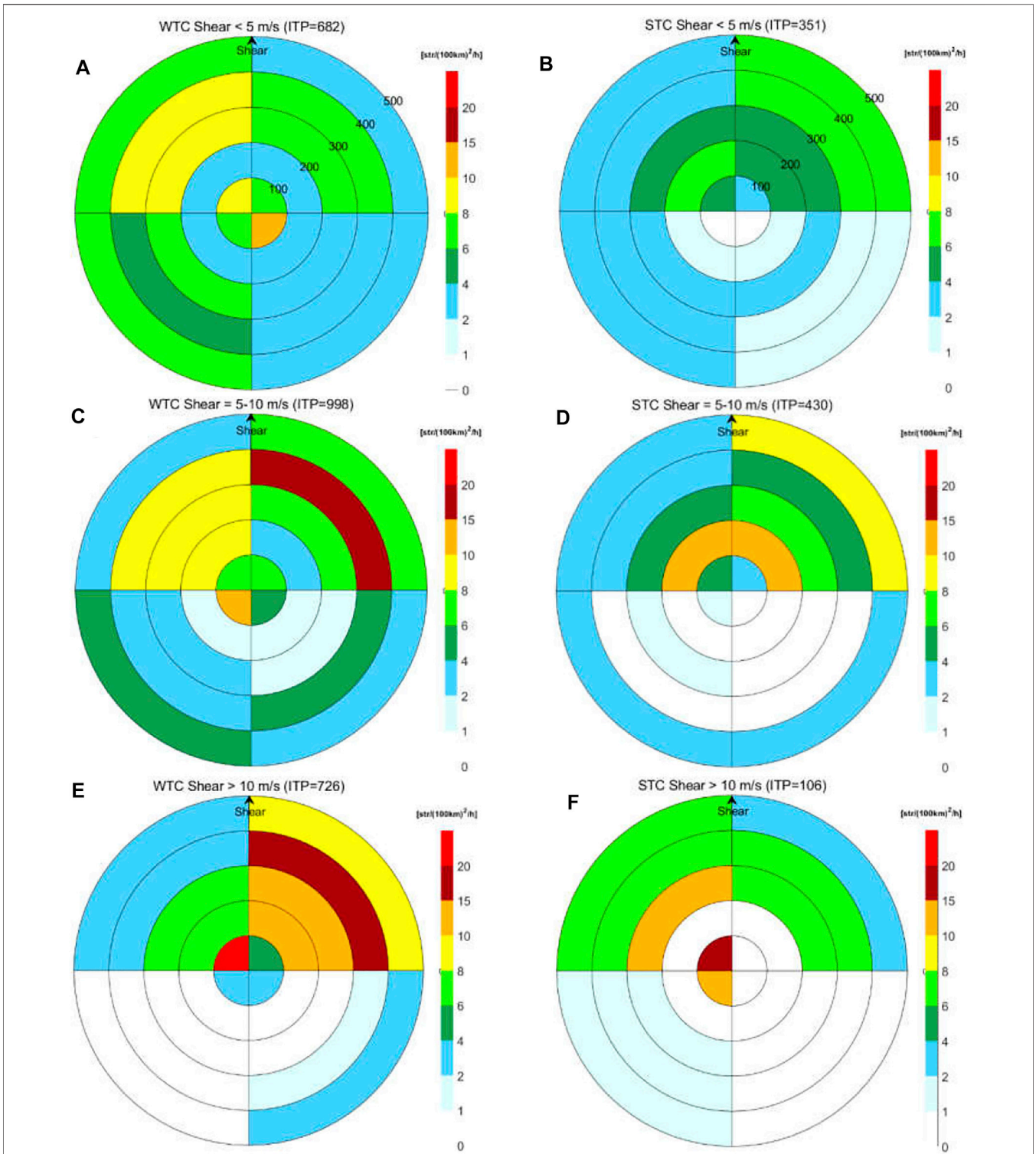

FIGURE 10 | Lightning asymmetry as a function of shear magnitude in WTCs and STCs. **(A,B)**: low shear (<5 m s^{-1}), **(C,D)**: moderate shear (5–10 m s^{-1}), **(E,F)**: high shear (>10 m s^{-1}).

primary circulation of the TC vortex. Strong storms, especially under a low shear environment, have a more organized primary circulation than weak storms. In this case, shear-induced asymmetry is less profound, and deep convections are more symmetrically distributed around the storm center. On the other hand, this might be due to the formation of a secondary

TABLE 4 | The favored quadrant and the magnitude of lightning asymmetry (relative to shear) as a function of landing locations. V_{max}, shear and motion are the mean values during the 48-h landfall period.

Location	ITP	Vmax (m/s)	Motion (m/s)	Shear (m/s)	Favored quadrant	Asymmetry magnitude
FJ	899	27.1	5.5	6.5	DL	4.33
GD	1254	25.9	5.5	7.5	DR	3.57
ZJSH	400	27.2	5.8	7.8	DR	4.92
HN	740	26.6	5.6	8.8	DL	5.48

eyewall during the restrengthening onshore. Using 6-year passive microwave imageries, Hawkins and Helveston (2004) found that approximately 80% of TCs in the western Pacific had double eyes and eyewall replacement cycles. Kuo et al. (2009) also found that 72% of major typhoons (category 5 typhoons) underwent concentric eyewalls (CEs) in the western North Pacific typhoons in 1997–2006. It is suggested that strong typhoons containing CE structure tend to occur farther west in the northwest Pacific. Furthermore, 42% of the samples of CE formation in their study occurred in the sea area west of 130°E (see **Figure 2** in Kuo et al., 2009), which is the domain of this study for landing TCs in China.

Figure 10 demonstrates the shear-relative lightning asymmetry by dividing WTC and STC samples into three subsets: low shear (<5 m s^{-1}), moderate shear (5–10 m s^{-1}), and high shear (>10 m s^{-1}). Lightning asymmetry increases with increasing shear magnitude in both WTCs and STCs. Lightning asymmetry is less pronounced in a low shear environment (**Figures 10A,B**), and the ratio of average lightning density is small between favored and unfavored quadrants. Such asymmetries are more significant in moderate and high shear environments (**Figures 10C,F**). When the shear magnitude is larger than 10 m s^{-1}, the outer rainband lightning is mainly concentrated in the DR quadrants, and the inner-core lightning is concentrated in the DL quadrant (**Figures 10E,F**). The quadrant-mean lightning densities are much lower for strong TCs than for weak TCs. Furthermore, WTCs tend to have broader deep convection areas in downshear quadrants in high shear environments, with lightning density >15 str $(100\ km)^{-1}$ h^{-1} in the 300–400 km radius (**Figure 10E**). Observational studies (Cecil, 2007; Xu et al., 2014; Yu et al., 2017; Pei and Jiang, 2018) on precipitation have found that TCs in strong vertical wind shear show significant asymmetries, with the maximum rainfall located in the downshear quadrants. Similar patterns are also observed in the lightning asymmetry distribution in this study.

Vertical wind shear dominates lightning asymmetries, particularly in a moderate to high sheared environment. In a low shear environment, the motion vector has a larger contribution than the shear vector, and the down motion left component is more important (Pei and Jiang, 2018). While when the shear becomes strong, intense convection and higher reflectivity will be found on the DL quadrant in TC asymmetry (Rogers et al., 2003). **Table 4** shows the favored quadrant and the magnitude of lightning asymmetry for all landing locations. It is clear that the asymmetry magnitude increases with the value of wind shear. The asymmetry magnitude is 4.33 under smaller shear conditions (6.5 m/s in FJ) and increases to 4.92 and 5.48 in ZJSH and HN, respectively, with larger shear values (7.8 and 8.8 m/s). The convective asymmetry is not significant when the TC is far from land. As it approaches the coastline, stronger convection and asymmetric distributions may develop in the region between the storm core and the land. Just during landfall, storm motion may partly explain the along-coast convective asymmetry, but vertical wind shear is the more dominant factor than storm motion. Such strong convection in downshear quadrants is due to the influences of environmental situations, differential forcing between land and ocean, local topographic effects, and dry air intrusion from the continent (Chan et al., 2004; Shu et al., 2018).

6 CONCLUSION

This study quantified the characteristics of lightning in tropical cyclones making landfall in China using 11 years of lightning data from the WWLLN during 2010–2020. A total of 3,293 individual time periods were collected in 79 landfalls from 74 TCs with intensities ranging from tropical storms to super typhoons. The landfall period is confined to 48 h from 24 h prior to landfall to 24 h after landfall. The statistics of TC lightning rates, including extremes and PDFs, are analyzed, and the radial distribution and evolution of lightning density during landfall are investigated. Lightning asymmetries relative to the vertical wind shear are constructed to examine the impacts of landing location, TC intensity and environmental vertical wind shear on convective asymmetries.

WWLLN detected lightning activity in *all TCs* in 2010–2020 during the 48-h landfall, with the highest lightning count in Tropical Storm Haitang (2017) and the lowest in Severe Tropical Storm Ampil (2018). Extreme inner-core lightning rates (>500 str h^{-1}) prefer to occur in low-latitude oceanic regions (south of 23°N) prior to TC landfall. Extreme lightning rates in the rainband region are comparable to lightning activity in mesoscale convection systems on land. High lightning rates seem more likely to occur in weaker storms at TS and STS intensities, indicating that weak TCs can produce intense lightning and deep convection during their landfall.

The PDF analysis reveals that TC hourly lightning rates are distributed between 1 and 4,447 str h^{-1} and most frequently appear between 250 and 600 str h^{-1}. Weak storms tend to have higher lightning rates during landfall than strong storms. TCs landing in Guangdong and Hainan have the largest peak lightning rates, while those landing in Zhejiang and Shanghai show the lowest lightning rates. The storms landing at Zhejiang

and Shanghai have higher intensity and the lower SST in the waters there inhibits strong convection and active lightning activity in these regions.

During the pre-landfall period, lightning density shows a maximum within 40 km from the storm center. It reaches the minimum at a radius of 120 km and then increases again in the outer rainbands. This radial structure of TC lightning prior to landfall is consistent with the lightning distribution in mature hurricanes (Molinari et al., 1994, 1999; DeMaria et al., 2012). In contrast, starting from landing to 24 h after landfall, lightning densities in all radii are decreased, and the maximum shifts to approximately 350 km from the center. The shift in the lightning maximum from the inner core to the outer rainbands reveals the effect of dry continental air intrusion and the enhanced surface frictional convergence during the landfall period. In addition, lightning density in weak storms decreases more sharply with radius compared to strong storms during the 48-h landfall.

The maximum lightning density is found in the inner core region in weak storms when they are located approximately 100–200 km away from the coastline. Moreover, lightning density within the inner core is positively related to TC wind speed, with a slight increase from 24 to 6 h (t_{-24}~t_{-6}) prior to landfall and a sharp decrease after landfall (t_0~t_{24}). In contrast, lightning density in the outer rainbands remains stable during the 48-h landfall.

This study also investigated the possible influences of vertical wind shear, landing location, and TC intensity on lightning and convective asymmetries. In agreement with Corbosiero and Molinari (2002) and Stevenson et al. (2016), our results suggest that vertical wind shear is a more important factor in producing TC lightning and convective asymmetry during landfall. The lightning maximum is found in the downshear left quadrant in the inner core and the downshear to downshear right quadrants in the outer rainbands. As the storms move onshore, approach the coast, and finally make landfall, intense convections rotate counterclockwise, and lightning asymmetries shift slightly cyclonically to the left.

WTCs (<32.7 m/s) show stronger lightning densities and larger maximum density areas. However, when weak storms intensify into STCs (≥32.7 m/s), the area of high lightning density markedly decreases, especially within the inner-core region. Strong axisymmetric lightning within the inner core in the STCs during pre-landfall is observed, which is possibly due to the more organized primary circulation and the formation of secondary eyewalls during the re-strengthening onshore. Lightning asymmetry increases with increasing shear magnitude in both WTCs and STCs. The asymmetry is less pronounced in low (<5 m s^{-1}) shear environments but more significant in moderate (5–10 m s^{-1}) and high (>10 m s^{-1}) shear environments. The lightning and convective asymmetries for landing TCs are more pronounced than those for TCs over waters, which is possibly due to the combined influences of environmental shear, differential forcing between land and ocean, local topographic effects, and dry air intrusion from the continent.

The results of this study could be used as a basis to improve our current knowledge of lightning and convective structure for TCs making landfall. The next step will be to investigate the favorable large-scale environments for TCs producing high lightning rates during landfall, especially the difference in dominant environmental conditions between the inner core and the outer rainbands to produce extreme high lightning rates in different TC regions.

DATA AVAILABILITY STATEMENT

The original contributions presented in the study are included in the article/Supplementary Material, further inquiries can be directed to the corresponding author.

AUTHOR CONTRIBUTIONS

Conceptualization, WZ and YZ; Formal analysis, WZ and SS; Data curation, WZ and DZ; Figures, WZ and LX; Draft writing, WZ, YZ, and SS.

FUNDING

This work is jointly supported by the National Key Research and Development Program of China (Grant 2019YFC1510103) and the Basic Research Fund of Chinese Academy of Meteorological Sciences (Grant 2020Z009).

REFERENCES

Abarca, S. F., Corbosiero, K. L., and Galarneau, T. J. (2010). An Evaluation of the Worldwide Lightning Location Network (WWLLN) Using the National Lightning Detection Network (NLDN) as Ground Truth. *J. Geophys. Res.* 115, D18206. doi:10.1029/2009JD013411

Abarca, S. F., Corbosiero, K. L., and Vollaro, D. (2011). The World Wide Lightning Location Network and Convective Activity in Tropical Cyclones. *Mon. Weather Rev.* 139, 175–191. doi:10.1175/2010mwr3383.1

Bovalo, C., Barthe, C., Yu, N., and Bègue, N. (2014). Lightning Activity within Tropical Cyclones in the South West Indian Ocean. *J. Geophys. Res. Atmos.* 119, 8231–8244. doi:10.1002/2014JD021651

Cecil, D. J., and Zipser, E. J. (1999). Relationships between Tropical Cyclone Intensity and Satellite-Based Indicators of Inner Core Convection: 85-GHz Ice-Scattering Signature and Lightning. *Mon. Weather Rev.* 127, 103–123. doi:10.1175/1520-0493(1999)127<0103:rbtcia>2.0.co;2

Cecil, D. J., Zipser, E. J., and Nesbitt, S. W. (2002). Reflectivity, Ice Scattering, and Lightning Characteristics of Hurricane Eyewalls and Rainbands. Part I: Quantitative Description. *Mon. Weather Rev.* 130, 769–784. doi:10.1175/1520-0493(2002)130<0769:risalc>2.0.co;2

Cecil, D. J. (2007). Satellite-derived Rain Rates in Vertically Sheared Tropical Cyclones. *Geophys. Res. Lett.* 34, L02811. doi:10.1029/2006GL027942

Chan, J. C. L., Liu, K. S., Ching, S. E., and Lai, E. S. T. (2004). Asymmetric Distribution of Convection Associated with Tropical Cyclones Making Landfall along the South China Coast. *Mon. Weather Rev.* 132, 2410–2420. doi:10.1175/1520-0493(2004)132<2410:adocaw>2.0.co;2

Chen, L., and Xu, Y. (2017). Review of Typhoon Very Heavy Rainfall in China. *Meteorol. Environ. Sci.* 40, 3–10. doi:10.16765/j.cnki.1673-7148.2017.01.001

Chien, F.-C., and Kuo, H.-C. (2011). On the Extreme Rainfall of Typhoon Morakot (2009). *J. Geophys. Res.* 116, D05104. doi:10.1029/2010JD015092

Corbosiero, K. L., and Molinari, J. (2002). The Effects of Vertical Wind Shear on the Distribution of Convection in Tropical Cyclones. *Mon. Weather Rev.* 130, 2110–2123. doi:10.1175/1520-0493(2002)130<2110:teovws>2.0.co;2

Corbosiero, K. L., and Molinari, J. (2003). The Relationship between Storm Motion, Vertical Wind Shear, and Convective Asymmetries in Tropical Cyclones. *J. Atmos. Sci.* 60, 366–376. doi:10.1175/1520-0469(2003)060<0366:trbsmv>2.0.co;2

DeMaria, M., DeMaria, R. T., Knaff, J. A., and Molenar, D. (2012). Tropical Cyclone Lightning and Rapid Intensity Change. *Mon. Weather Rev.* 140, 1828–1842. doi:10.1175/mwr-d-11-00236.1

Duran, P., Schultz, C. J., Bruning, E. C., Stevenson, S. N., PeQueen, D. J., Johnson, N. E., et al. (2021). The Evolution of Lightning Flash Density, Flash Size, and Flash Energy during Hurricane Dorian's (2019) Intensification and Weakening. *Geophys. Res. Lett.* 48, e2020GL092067. doi:10.1029/2020GL092067

Fierro, A. O., Shao, X.-M., Hamlin, T., Reisner, J. M., and Harlin, J. (2011). Evolution of Eyewall Convective Events as Indicated by Intracloud and Cloud-To-Ground Lightning Activity during the Rapid Intensification of Hurricanes Rita and Katrina. *Mon. Weather Rev.* 139, 1492–1504. doi:10.1175/2010mwr3532.1

Fierro, A. O., Stevenson, S. N., and Rabin, R. M. (2018). Evolution of GLM-Observed Total Lightning in Hurricane Maria (2017) during the Period of Maximum Intensity. *Mon. Weather Rev.* 146, 1641–1666. doi:10.1175/mwr-d-18-0066.1

Goodman, S. J., Blakeslee, R. J., Koshak, W. J., Mach, D., Bailey, J., Buechler, D., et al. (2013). The GOES-R Geostationary Lightning Mapper (GLM). *Atmos. Res.* 125-126, 34–49. doi:10.1016/j.atmosres.2013.01.006

Gray, W. M. (1968). Global View of the Origin of Tropical Disturbances and Storms. *Mon. Weather Rev.* 96, 669–700. doi:10.1175/1520-0493(1968)096<0669:gvotoo>2.0.co;2

Hawkins, J. D., and Helveston, M. (2004). "Tropical Cyclone Multiple Eyewall Characteristics," in 26th Conference on Hurricane and Tropical Meteorology. Miami, FL; Date: 3-7 May 2004 (Miami, FL: American Meteorological Society), 1–7.

Holzworth, R. H., McCarthy, M. P., Brundell, J. B., Jacobson, A. R., and Rodger, C. J. (2019). Global Distribution of Superbolts. *JGR Atmos.* 124, 9996–10005. doi:10.1029/2019JD030975

Holzworth, R. H., Brundell, J. B., McCarthy, M. P., Jacobson, A. R., Rodger, C. J., and Anderson, T. S. (2021). Lightning in the Arctic. *Geophys. Res. Lett.* 48, e2020GL091366. doi:10.1029/2020GL091366

Houze, R. A. (2010). Clouds in Tropical Cyclones. *Mon. Weather Rev.* 138, 293–344. doi:10.1175/2009mwr2989.1

Hui, W., Zhang, W., Lyu, W., and Li, P. (2020). Preliminary Observations from the China fengyun-4A Lightning Mapping Imager and its Optical Radiation Characteristics. *Remote Sens.* 12, 2622. doi:10.3390/rs12162622

Jacobson, A. R., Holzworth, R., Harlin, J., Dowden, R., and Lay, E. (2006). Performance Assessment of the World Wide Lightning Location Network (WWLLN), Using the Los Alamos Sferic Array (LASA) as Ground Truth. *J. Atmos. Ocean. Technol.* 23, 1082–1092. doi:10.1175/jtech1902.1

Jiang, H., Ramirez, E. M., and Cecil, D. J. (2013). Convective and Rainfall Properties of Tropical Cyclone Inner Cores and Rainbands from 11 Years of TRMM Data. *Mon. Weather Rev.* 141, 431–450. doi:10.1175/mwr-d-11-00360.1

Kong, X., Zhao, Y., Qiu, Z., Tao, X., and Zhang, W. (2021). A Simple Method for Predicting Intensity Change Using the Peak Time Lag between Lightning and Wind in Tropical Cyclones. *Geophys. Res. Lett.* 48, e2020GL088872. doi:10.1029/2020GL088872

Kuo, H.-C., Chang, C.-P., Yang, Y.-T., and Jiang, H.-J. (2009). Western North Pacific Typhoons with Concentric Eyewalls. *Mon. Weather Rev.* 137, 3758–3770. doi:10.1175/2009mwr2850.1

Leary, L. A., and Ritchie, E. A. (2009). Lightning Flash Rates as an Indicator of Tropical Cyclone Genesis in the Eastern North Pacific. *Mon. Weather Rev.* 137, 3456–3470. doi:10.1175/2009mwr2822.1

Lin, S.-J., and Chou, K.-H. (2020). The Lightning Distribution of Tropical Cyclones over the Western North Pacific. *Mon. Weather Rev.* 148, 4415–4434. doi:10.1175/mwr-d-19-0327.1

Liu, D., Sun, M., Su, D., Xu, W., Yu, H., and Chen, Y. (2021). A Five-Year Climatological Lightning Characteristics of Linear Mesoscale Convective Systems over North China. *Atmos. Res.* 256, 105580. doi:10.1016/j.atmosres.2021.105580

Molinari, J., Moore, P. K., Idone, V. P., Henderson, R. W., and Saljoughy, A. B. (1994). Cloud-to-ground Lightning in Hurricane Andrew. *J. Geophys. Res.* 99, 16665–16676. doi:10.1029/94JD00722

Molinari, J., Moore, P., and Idone, V. (1999). Convective Structure of Hurricanes as Revealed by Lightning Locations. *Mon. Weather Rev.* 127, 520–534. doi:10.1175/1520-0493(1999)127<0520:csohar>2.0.co;2

Molinari, J., Vollaro, D., and Corbosiero, K. L. (2004). Tropical Cyclone Formation in a Sheared Environment: A Case Study. *J. Atmos. Sci.* 61, 2493–2509. doi:10.1175/jas3291.1

Molinari, J., Dodge, P., Vollaro, D., Corbosiero, K. L., and Marks, F. (2006). Mesoscale Aspects of the Downshear Reformation of a Tropical Cyclone. *J. Atmos. Sci.* 63, 341–354. doi:10.1175/jas3591.1

Pan, L., Qie, X., Liu, D., Wang, D., and Yang, J. (2010). The Lightning Activities in Super Typhoons over the Northwest Pacific. *Sci. China Earth Sci.* 53, 1241–1248. doi:10.1007/s11430-010-3034-z

Pan, L., Qie, X., and Wang, D. (2014). Lightning Activity and its Relation to the Intensity of Typhoons over the Northwest Pacific Ocean. *Adv. Atmos. Sci.* 31, 581–592. doi:10.1007/s00376-013-3115-y

Pei, Y., and Jiang, H. (2018). Quantification of Precipitation Asymmetries of Tropical Cyclones Using 16-Year TRMM Observations. *J. Geophys. Res. Atmos.* 123, 8091–8114. doi:10.1029/2018JD028545

Price, C., Asfur, M., and Yair, Y. (2009). Maximum Hurricane Intensity Preceded by Increase in Lightning Frequency. *Nat. Geosci.* 2, 329–332. doi:10.1038/ngeo477

Ringhausen, J. S., and Bitzer, P. M. (2021). An In-Depth Analysis of Lightning Trends in Hurricane Harvey Using Satellite and Ground-Based Measurements. *Geophys Res. Atmos.* 126, e2020JD032859. doi:10.1029/2020JD032859

Rodger, C. J., Werner, S., Brundell, J. B., Lay, E. H., Thomson, N. R., Holzworth, R. H., et al. (2006). Detection Efficiency of the VLF World-wide Lightning Location Network (WWLLN): Initial Case Study. *Ann. Geophys.* 24, 3197–3214. doi:10.5194/angeo-24-3197-2006

Rogers, R., Chen, S., Tenerelli, J., and Willoughby, H. (2003). A Numerical Study of the Impact of Vertical Shear on the Distribution of Rainfall in Hurricane Bonnie (1998). *Mon. Weather Rev.* 131, 1577–1599. doi:10.1175//2546.1

Rudlosky, S. D., and Shea, D. T. (2013). Evaluating WWLLN Performance Relative to TRMM/LIS. *Geophys. Res. Lett.* 40, 2344–2348. doi:10.1002/grl.50428

Samsury, C. E., and Orville, R. E. (1994). Cloud-to-ground Lightning in Tropical Cyclones: A Study of Hurricanes Hugo (1989) and Jerry (1989). *Mon. Weather Rev.* 122, 1887–1896. doi:10.1175/1520-0493(1994)122<1887:ctglit>2.0.co;2

Shao, X.-M., Harlin, J., Stock, M., Stanley, M., Regan, A., Wiens, K., et al. (2005). Katrina and Rita Were Lit up with Lightning. *Eos Trans. AGU* 86, 398. doi:10.1029/2005EO420004

Shu, S., Feng, X., and Wang, Y. (2018). Essential Role of Synoptic Environment on Rainfall Distribution of Landfalling Tropical Cyclones over China. *J. Geophys. Res. Atmos.* 123, 285–311. doi:10.1029/2018JD028842

Solorzano, N., Thomas, J., and Bracy, C. (2018). Monitoring Tropical Cyclones with Lightning and Satellite Data. *EOS* 99. doi:10.1029/2018EO092439

Squires, K., and Businger, S. (2008). The Morphology of Eyewall Lightning Outbreaks in Two Category 5 Hurricanes. *Mon. Weather Rev.* 136, 1706–1726. doi:10.1175/2007mwr2150.1

Stevenson, S. N., Corbosiero, K. L., and Molinari, J. (2014). The Convective Evolution and Rapid Intensification of Hurricane Earl (2010). *Mon. Weather Rev.* 142, 4364–4380. doi:10.1175/mwr-d-14-00078.1

Stevenson, S. N., Corbosiero, K. L., and Abarca, S. F. (2016). Lightning in Eastern North Pacific Tropical Cyclones: A Comparison to the North Atlantic. *Mon. Weather Rev.* 144, 225–239. doi:10.1175/mwr-d-15-0276.1

Stevenson, S. N., Corbosiero, K. L., DeMaria, M., and Vigh, J. L. (2018). A 10-year Survey of Tropical Cyclone Inner-Core Lightning Bursts and Their Relationship to Intensity Change. *Weather Forecast* 33, 23–36. doi:10.1175/waf-d-17-0096.1

Susca-Lopata, G., Zawislak, J., Zipser, E. J., and Rogers, R. F. (2015). The Role of Observed Environmental Conditions and Precipitation Evolution in the Rapid Intensification of Hurricane Earl (2010). *Mon. Weather Rev.* 143, 2207–2223. doi:10.1175/mwr-d-14-00283.1

Thomas, J. N., Solorzano, N. N., Cummer, S. A., and Holzworth, R. H. (2010). Polarity and Energetics of Inner Core Lightning in Three Intense North Atlantic Hurricanes. *J. Geophys. Res.* 115, A00E15. doi:10.1029/2009JA014777

Vagasky, C. (2017). Enveloped Eyewall Lightning: the EEL Signature in Tropical Cyclones. *J. Oper. Meteor.* 05, 171–179. doi:10.15191/nwajom.2017.0514

Virts, K. S., Wallace, J. M., Hutchins, M. L., and Holzworth, R. H. (2013). Highlights of a New Ground-Based, Hourly Global Lightning Climatology. *Bull. Amer. Meteor. Soc.* 94, 1381–1391. doi:10.1175/bams-d-12-00082.1

Wang, F., Qie, X., Liu, D., Shi, H., and Srivastava, A. (2016). Lightning Activity and its Relationship with Typhoon Intensity and Vertical Wind Shear for Super Typhoon Haiyan (1330). *J. Meteorol. Res.* 30, 117–127. doi:10.1007/s13351-016-4228-x

Wang, F., Qie, X., Wang, D., and Srivastava, A. (2018). Lightning Activity in Tropical Cyclones and its Relationship to Dynamic and Thermodynamic Parameters over the Northwest Pacific. *Atmos. Res.* 213, 86–96. doi:10.1016/j.atmosres.2018.05.027

Whittaker, I. C., Douma, E., Rodger, C. J., and Marshall, T. J. C. H. (2015). A Quantitative Examination of Lightning as a Predictor of Peak Winds in Tropical Cyclones. *J. Geophys. Res. Atmos.* 120, 3789–3801. doi:10.1002/2014JD022868

Williams, E. R. (1988). The Electrification of Thunderstorms. *Sci. Am.* 259, 88–99. doi:10.1038/scientificamerican1188-88

Xia, R., Zhang, D.-L., and Wang, B. (2015). A 6-yr Cloud-To-Ground Lightning Climatology and its Relationship to Rainfall over Central and Eastern China. *J. Appl. Meteorol. Climatol.* 54, 2443–2460. doi:10.1175/jamc-d-15-0029.1

Xu, W., Jiang, H., and Kang, X. (2014). Rainfall Asymmetries of Tropical Cyclones Prior to, during, and after Making Landfall in South China and Southeast United States. *Atmos. Res.* 139, 18–26. doi:10.1016/j.atmosres.2013.12.015

Xu, W., Rutledge, S. A., and Zhang, W. (2017). Relationships between Total Lightning, Deep Convection, and Tropical Cyclone Intensity Change. *J. Geophys. Res. Atmos.* 122, 7047–7063. doi:10.1002/2017JD027072

Yokoyama, C., and Takayabu, Y. N. (2008). A Statistical Study on Rain Characteristics of Tropical Cyclones Using TRMM Satellite Data. *Mon. Wea. Rev.* 136, 3848–3862. doi:10.1175/2008mwr2408.1

Yu, Z., Wang, Y., Xu, H., Davidson, N., Chen, Y., Chen, Y., et al. (2017). On the Relationship between Intensity and Rainfall Distribution in Tropical Cyclones Making Landfall over China. *J. Appl. Meteorol. Climatol.* 56, 2883–2901. doi:10.1175/jamc-d-16-0334.1

Zhang, W., Zhang, Y., Zheng, D., and Zhou, X. (2012). Lightning Distribution and Eyewall Outbreaks in Tropical Cyclones during Landfall. *Mon. Weather Rev.* 140, 3573–3586. doi:10.1175/mwr-d-11-00347.1

Zhang, W., Zhang, Y., Zheng, D., Wang, F., and Xu, L. (2015). Relationship between Lightning Activity and Tropical Cyclone Intensity over the Northwest Pacific. *J. Geophys. Res. Atmos.* 120, 4072–4089. doi:10.1002/2014JD022334

Zhang, W., Hui, W., Lyu, W., Cao, D., Li, P., Zheng, D., et al. (2020a). FY-4A LMI Observed Lightning Activity in Super Typhoon Mangkhut (2018) in Comparison with WWLLN Data. *J. Meteorol. Res.* 34, 336–352. doi:10.1007/s13351-020-9500-4

Zhang, W., Zhang, Y., Zheng, D., and Lyu, W. (2020b). Quantifying the Contribution of Tropical Cyclones to Lightning Activity over the Northwest Pacific. *Atmos. Res.* 239, 104906. doi:10.1016/j.atmosres.2020.104906

Conflict of Interest: The authors declare that the research was conducted in the absence of any commercial or financial relationships that could be construed as a potential conflict of interest.

Publisher's Note: All claims expressed in this article are solely those of the authors and do not necessarily represent those of their affiliated organizations, or those of the publisher, the editors and the reviewers. Any product that may be evaluated in this article, or claim that may be made by its manufacturer, is not guaranteed or endorsed by the publisher.

Copyright © 2022 Zhang, Zhang, Shu, Zheng and Xu. This is an open-access article distributed under the terms of the Creative Commons Attribution License (CC BY). The use, distribution or reproduction in other forums is permitted, provided the original author(s) and the copyright owner(s) are credited and that the original publication in this journal is cited, in accordance with accepted academic practice. No use, distribution or reproduction is permitted which does not comply with these terms.